



OPEN

Tensile strain and altered synovial tissue metabolism in human knee osteoarthritis

Holly T. Philpott^{1,2}, Trevor B. Birmingham^{1,2}, Benoit Fiset³, Logan A. Walsh^{3,4}, Mitchell C. Coleman^{5,6}, Cheryle A. Séguin^{2,7} & C. Thomas Appleton^{2,7,8,9}✉

Synovium is critical for maintaining joint homeostasis and may contribute to mechanobiological responses during joint movement. We investigated mechanobiological responses of whole synovium from patients with late-stage knee osteoarthritis (OA). Synovium samples were collected during total knee arthroplasty and assigned to histopathology or cyclic 10% tensile strain loading, including (1) static (control); (2) low-frequency (0.3 Hz); and (iii) high-frequency (1.0 Hz) for 30-min. After 6-h incubation, tissues were bisected for RNA isolation and immunostaining (3-nitrotyrosine; 3-NT). RNA sequencing was analyzed for differentially expressed genes and pathway enrichment. Cytokines and lactate were measured in conditioned media. Compared to controls, low-frequency strain induced enrichment of pathways related to interferon response, Fc-receptor signaling, and cell metabolism. High-frequency strain induced enrichment of pathways related to NOD-like receptor signaling, high metabolic demand, and redox signaling/stress. Metabolic and redox cell stress was confirmed by increased release of lactate into conditioned media and increased 3-NT formation in the synovial lining. Late-stage OA synovial tissue responses to tensile strain include frequency-dependent increases in inflammatory signaling, metabolism, and redox biology. Based on these findings, we speculate that some synovial mechanobiological responses to strain may be beneficial, but OA likely disturbs synovial homeostasis leading to aberrant responses to mechanical stimuli, which requires further validation.

The synovium is vital for joint homeostasis and experiences tensile and convective forces during flexion–extension joint movements^{1,2}; synovial physiologic responses to mechanical loading may therefore help or worsen joint outcomes in osteoarthritis (OA). Although healthy synovium delivers nutrients and produces lubricating molecules³, OA induces marked changes in synovial tissues, which impair joint homeostasis and exacerbate pathogenesis^{3,4}. Synovial inflammation predicts worse clinical outcomes in patients with knee OA^{5–10}. Therefore, identifying the synovial biological mechanisms involved in OA pathogenesis is critical for developing new disease-modifying therapies for this debilitating disease.

Although a great deal is known about the effects of mechanical loading on cartilage, little research exists on mechanical loading in synovial tissues. Mechanical stresses on articular cartilage invoke inflammatory, redox, and metabolic changes in cellular physiology, which influence OA pathogenesis¹¹ and could similarly disrupt synovial function directly, and/or through crosstalk between cartilage and synovium. Recent descriptions of biological crosstalk between synovial cells and chondrocytes¹² demonstrate the importance of considering synovial biology in addition to OA-driven cartilage degradation.

A paradoxical relationship exists between OA and physical activity. Physical activity or exercise improves joint pain and function in the medium to long-term^{13,14}, but many patients experience pain, stiffness, and joint inflammation during physical activity, and acute improvement with rest^{15–17}. This suggests that differences exist

¹Faculty of Health Sciences, Western University, London, ON N6G 1H1, Canada. ²Bone and Joint Institute, Western University, London, ON N6A 5B5, Canada. ³Rosalind and Morris Goodman Cancer Research Centre, McGill University, Montreal, QC H3A 1A3, Canada. ⁴Department of Human Genetics, McGill University, Montreal, QC H3A 0C7, Canada. ⁵Department of Orthopedics and Rehabilitation, University of Iowa, Iowa City, IA 52242, USA. ⁶Department of Radiation Oncology, University of Iowa, Iowa City, IA 52242, USA. ⁷Department of Physiology and Pharmacology, Schulich School of Medicine and Dentistry, Western University, London, ON N6A 5C1, Canada. ⁸Department of Medicine, Schulich School of Medicine and Dentistry, Western University, London, ON N6A 5C1, Canada. ⁹SJHC Rheumatology Centre, 268 Grosvenor St., London, ON N6A 4V2, Canada. ✉email: tom.appleton@sjhc.london.on.ca

Characteristic	All patients (n = 10)	RNA sequencing sub-group (n = 6)
Age, years	67.4 ± 7.9 [54–77]	66.3 ± 9.5 [54–77]
Sex, n (%)		
Female	4 (40.0%)	2 (33.3%)
Male	6 (60.0%)	4 (66.7%)
BMI, (kg/m ²)	35.5 ± 6.1 [29.5–45.4]	36.1 ± 5.6 [29.5–44.6]
KL grade, n (%)		
Grade 3	3 (30.0%)	1 (16.7%)
Grade 4	7 (70.0%)	5 (83.3%)
KOOS Pain subscale, (0–100)	39.6 ± 22.2 [0–67]	39.5 ± 24.5 [0–67]
Histopathology, mean score		
Synovial Lining thickness	0.7 ± 0.4 [0.4–1.6]	0.6 ± 0.4 [0.4–1.0]
Sub-synovial infiltrate	1.2 ± 0.7 [0.6–2.4]	1.3 ± 0.6 [0.6–2.2]
Fibrin Deposition	0.8 ± 0.3 [0–1]	0.8 ± 0.4 [0–1]
Vascularization	1.8 ± 0.9 [0–3.0]	1.7 ± 1.2 [0–3.0]
Fibrosis	1.3 ± 0.6 [0.6–2.5]	1.4 ± 0.5 [0.6–2.5]
Perivascular edema	0.7 ± 0.6 [0–1.6]	0.8 ± 0.8 [0–1.6]
Comorbidities, n (%)		
Hypertension	8 (80.0%)	4 (66.7%)
Dyslipidemia	6 (60.0%)	3 (50.0%)
Diabetes (Type II)	4 (40.0%)	2 (33.3%)
Obesity	7 (70.0%)	5 (83.3%)
Smoking		
Active	0 (0.0%)	0 (0.0%)
Previous	2 (20.0%)	1 (16.7%)
Chronic liver disease	0 (0.0%)	0 (0.0%)
Chronic kidney disease	0 (0.0%)	0 (0.0%)

Table 1. Patient demographics, clinical characteristics and synovial histopathology. Mean ± SD (minimum, maximum) or n (%). BMI, body mass index; KL, Kellgren-Lawrence grade; KOOS, Knee Injury and Osteoarthritis Outcome Score.

in the mechanisms mediating the short-term, versus medium- to long-term effects of physical activity. Given recent discoveries underscoring the key relationship of the synovium to joint outcomes^{5–10}, especially pain, we propose that OA synovium may display aberrant physiologic responses to mechanical stimuli, which in turn could contribute to OA pathogenesis, disease progression, and worse patient outcomes.

A recent study characterized the compressive properties and permeability of healthy synovium¹⁸. However, a major gap remains in our understanding of the mechanobiology of OA synovium. Importantly, tensile strain loading of synovial cells in vitro has been shown to induce changes in extracellular matrix, inflammatory, and oxidative stress gene expression^{19–22}, all of which could impact joint health and homeostasis. Therefore, our objective was to assess the physiologic responses of intact human synovial tissues to mechanical loading with cyclic tensile strain. We investigated synovial tissue responses in the clinical context of patients with late-stage knee OA, who are most likely to have physical activity-related symptoms. Since macrophages are the most abundant immune cell type in OA synovium^{23,24}, we also explored whether macrophage content in the synovial lining modifies the response to mechanical load.

Results

Synovial tissue samples were collected sequentially from 10 patients undergoing TKA recruited consecutively from January 2019 to July 2019. For RNA sequencing, we included n = 6 patients with synovial tissue RNA samples that met RNA quality/quantity requirements. Baseline demographics, clinical characteristics, and synovial histopathology for all 10 patients and the sub-group of 6 patients included for RNA sequencing are presented in Table 1.

OA synovial tissue transcriptomic responses to cyclic tensile strain. *Significantly dysregulated genes.* We explored differential gene expression induced by cyclic tensile strain in synovial tissues (Fig. 1). Compared to static control tissues, 1543 genes were significantly differentially expressed in OA synovial tissue after low-frequency tensile strain. Of these, 1463 genes decreased, 80 genes increased, and 1021 (66.2%) corresponded to non-coding genes. High-frequency strain induced differential expression of 101 genes, with 77 genes decreased, 24 genes increased, and 73 (72.3%) genes were non-coding. Only 27 genes were differentially expressed in both low- and high-frequency tensile strain conditions (Fig. 1a).

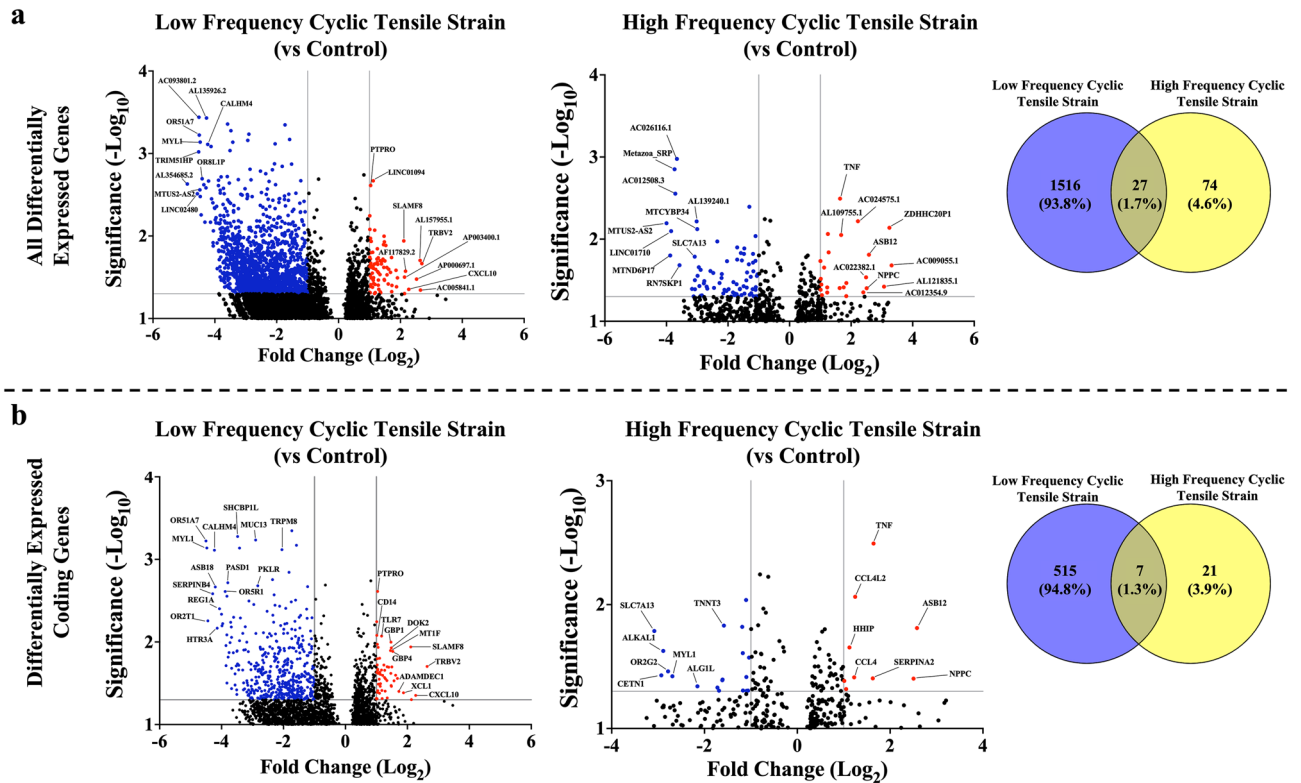


Figure 1. Differentially expressed genes in Low- and High-frequency tensile strain conditions (versus Control). (a) All differentially expressed genes and (b) differentially expressed coding genes. Each panel contains volcano plots displaying the top differentially expressed genes for low frequency cyclic tensile strain (vs control) and high frequency cyclic tensile strain (vs control). The Y-axis represents the $-\log_{10}$ p-value cut-off set at 1.3 (p -value < 0.05) and the X-axis represents the \log_2 fold change cut-off of below -1.0 (blue) or above 1.0 (red). Venn diagrams display the number of differentially expressed genes in common and unique to Low and High-frequency tensile strain conditions.

Of the 522 coding genes that were differentially expressed following low-frequency tensile strain (vs. control), 467 coding genes decreased, and 55 genes increased (Fig. 1b). Genes involved in circadian rhythm (*PASD1*), cell metabolism (*CALHM4*, *PKLR*, *G6PC2*), pain signaling (*TRPM8*, *HTR3A*), innate immunity (*REG1A*, *ASB18*), and the olfactory receptor gene family (*OR51A7*, *OR5R1*, *OR2T1*) were decreased, whereas genes involved in immune regulation (*CD14*, *CXCL10*, *TRBV2*, *DOK2*, *XCL1*, *ADAMDEC1*, *PTPRO*, *SLAMF8*) and cell metabolism (*MT1F*, *GBP1*, *GBP4*) were increased.

Of the 28 coding genes significantly differentially expressed following high-frequency tensile strain (vs. control), 19 genes decreased and 9 increased (Fig. 1b). Genes involved in transmembrane transport (*SLC7A13*), protein glycosylation (*ALGIL*), and the olfactory receptor gene family (*OR2G2*) were decreased, whereas genes involved in immune response (*TNF*, *CCL4*, *CCL4L2*, *SERPINA2*, *ASB12*), cell stress (*NPPC*), and hedgehog signaling (*HHIP*) were increased.

The 7 coding genes that were differentially expressed following both low- and high-frequency tensile strain (vs. control) are involved in cytoskeleton organization, microtubule organization, cellular component assembly, and nucleotide-excision repair (*CETN1*, *DIRAS3*, *EVA1A*, *LRRN1*, *MYL1*, *TNNT3*, *XIRP1*) (Fig. 1b).

Gene set enrichment analysis. Hallmark gene sets The top 10 significantly enriched Hallmark gene sets following exposure of OA synovial tissue to low-frequency, or high-frequency tensile strain (vs. control) are shown in Table 2. 43 gene sets were enriched by low-frequency tensile strain, including the same 26 gene sets significantly enriched by high-frequency tensile strain. Overall, cyclic tensile strain led to enrichment in gene sets related to inflammation (including TNF- α signaling via NF κ B, interferon gamma and alpha responses), metabolism (including adipogenesis, glycolysis, oxidative phosphorylation), and cell stress (including hypoxia, apoptosis, and p53 pathway) (Supplementary File 1). Interestingly, high-frequency tensile strain primarily led to enrichment in cell metabolism (fatty acid metabolism, adipogenesis, and xenobiotic metabolism) with nominally higher normalized enrichment scores relative to low-frequency tensile strain (Table 2). We therefore conducted a more detailed analysis of cellular metabolism gene sets using Reactome.

Reactome gene sets Compared to controls, low-frequency tensile strain led to significant positive enrichment of 493 gene sets, while high-frequency tensile strain significantly enriched 97 gene sets. Low-frequency tensile strain induced enrichment of immune activation processes (e.g., Fc receptor signalling pathways), while high-frequency tensile strain induced enrichment of more damaging immune responses (e.g., NOD-signalling, neutrophil degranulation, NF κ B translocation to nucleus, and NLR signaling pathways). There were 5 gene

HALLMARK: low-frequency strain versus control		
Gene set	NES	FDR q-val
Interferon gamma response	4.18	<0.0001
Interferon alpha response	4.00	<0.0001
Protein secretion	3.62	<0.0001
Oxidative phosphorylation	3.49	<0.0001
Allograft rejection	3.27	<0.0001
TNF- α signaling via NF κ B	3.19	<0.0001
Apoptosis	3.09	<0.0001
Inflammatory response	3.02	<0.0001
Adipogenesis	2.93	<0.0001
Hypoxia	2.82	<0.0001
HALLMARK: High-frequency strain versus control		
Gene set	NES	FDR q-val
Protein Secretion	2.55	<0.0001
Oxidative Phosphorylation	2.27	<0.0001
Inflammatory Response	2.24	<0.0001
TNF- α Signaling via NF κ B	2.19	<0.0001
Allograft Rejection	2.09	<0.0001
Hypoxia	2.05	<0.0001
Fatty Acid Metabolism	2.03	<0.0001
Apoptosis	2.01	<0.0001
Adipogenesis	1.96	<0.0001
Xenobiotic Metabolism	1.88	0.001

Table 2. Top 10 Enriched Hallmark gene sets for low and high frequency tensile strain. FDR, false discovery rate; NES, normalized enrichment score.

REACTOME: exclusive to high-frequency strain		
Gene set	NES	FDR q-value
Glyoxylate metabolism and glycine degradation	2.02	0.01
Metabolic Disorders of biological oxidation enzymes	2.00	0.01
Cytochrome P450 Arranged by Substrate Type	1.98	0.01
Respiratory ETC ATP Synthesis by Chemiosmotic Coupling and Heat Production by Uncoupling Proteins	1.83	0.03
Macroautophagy	1.82	0.03
Fatty Acids	1.76	0.03
Citric Acid Cycle/TCA Cycle	1.75	0.03
ER Quality Control Compartment ERQC	1.75	0.03
Diseases of Metabolism	1.73	0.04
Endogenous Sterols	1.69	0.04

Table 3. Metabolism-related Gene sets from Reactome exclusively enriched following high-frequency tensile strain. FDR, false discovery rate; NES, normalized enrichment score.

sets negatively enriched following low-frequency tensile strain related to cellular organization (keratinization, formation of cornified envelope), the mucin gene family, metabolism of amine-derived hormones, and olfactory signaling pathway, whereas no gene sets were negatively enriched in high-frequency tensile strain. Several significantly enriched gene sets related to cell metabolism and redox biology were exclusive to high-frequency tensile strain (Table 3). These included glyoxylate metabolism and glycine degradation, metabolic disorders of biological oxidation enzymes, macroautophagy, metabolism of fatty acids, citric acid cycle, diseases of metabolism, cytochrome P450, and others related to high levels of oxidative stress. The full lists of enriched Reactome gene sets can be found in Supplementary File 2.

Leading edge analysis. Leading edge analysis of significantly enriched cell metabolism and cell stress gene sets identified different top genes involved in enrichment following high- and low-frequency strain (Table 4). Leading edge genes following exposure to high-frequency tensile strain (vs control) included antioxidant genes for handling iron, superoxide, and nitric oxide (*FDX*, *DLD*, *SOD2*), AMPK-related genes (*PRKAB2*, *PRKAG2*,

Low vs control	High vs control	Low vs high	High vs low
UBC	CYC5	RPS27A	CYP1A2
UBB	SOD2	UBB	CYP2A13
GLB1	FDXR	UBA52	CYP4F22
RPS27A	PRKAB2	UBC	CYP2J2
CTSA	FDX1	DLD	UGT1A1
UBA52	FDX2	SDHC	UGT1A4
GYG1	PRKAG2	SDHD	
PRKAB2	PGM2L1	SDHA	
HEXB	DLD	MLST8	
HEXA	PRKAA2	ATP5F1B	

Table 4. Top Reactome leading edge genes related to cell stress, ROS, NOS, and cell metabolism gene sets enriched by low- or high-frequency (vs. control), or low- vs high-frequency tensile strain.

PRKAA2) responsible for regulating energy homeostasis and cell survival, genes related to galactose metabolism (*PGM2L1*) and reduction of P450 enzymes (*FDX*) Following exposure to low-frequency tensile strain (vs control), we identified leading edge genes related to lipid metabolism and T-cell activation (*HEXA*, *HEXB*), lysosomal routing, stability, and activation (*GLB1*, *CTSA*²⁵), and stimulation of proteasomal activity and/or mitophagy (*UBB*, *UBA52*, *UBC*). In tissues exposed to high-frequency strain (vs low-frequency) leading-edge identified *CYP* and *UGT* genes, which are activated by excess metabolite build up and by-products of severe oxidation^{26–28}. Leading edge genes for gene sets enriched by low-frequency strain (vs high-frequency) included *RPS27A*, ubiquitin genes (*UBB*, *UBA52*, *UBC*), *MLST8*, and *ATP5F1B*, which indicate stimulation of protein turnover and mitophagy^{29,30}.

Changes in lactate and cytokine/chemokine release into conditioned media following cyclic tensile strain. Since gene sets associated with metabolic disturbances and oxidative stress were enriched following cyclic tensile strain, we compared lactate and cytokine/chemokine release from synovial tissues in conditioned media after tensile strain loading (Fig. 2). Cyclic tensile strain increased lactate production (Fig. 2a). High-frequency strain increased synovial tissue lactate release (442.11 nmol [95%CI 73.15, 811.06]) compared to static controls (Fig. 2c). A small, statistically non-significant increase in lactate release was induced by low-frequency tensile strain (79.56 nmol [95%CI – 289.40, 448.51]) compared to static control (Fig. 2c).

MCP-1 concentration was highest in the conditioned media from control tissues (Fig. 2b). Tissues exposed to low-frequency strain had decreased MCP-1 release (– 3075.01 pg/mL [95%CI – 5201.69, – 948.33]) compared to control (Fig. 2c). A similar trend was seen with tissues exposed to high-frequency strain (– 2059.60 [95%CI – 4186.28, 67.08]) compared to control (Fig. 2c); however, this estimate lacked precision.

Mechanical strain induces oxidation in synovial tissue. Since our transcriptomics analysis identified strain-induced enrichment of numerous gene sets associated with oxidative stress, we measured 3-NT formation in synovial tissues (Fig. 3). 3-NT increases under oxidative stress because of increased reactions between superoxide and nitric oxide and is an indicator of excess superoxide production and inflammation-associated increases in nitric oxide. Static control OA synovial tissues demonstrated a small amount of 3-NT staining in 6 out of 10 patients. High-frequency tensile strain led to an increase in percent 3-NT positive synovial intima lining cells (16.83 [95%CI 1.87, 31.79]) compared to static control, while there was no clear change in 3-NT positive intimal cells following exposure to low-frequency strain (0.41 [95%CI – 14.55, 15.37]) (Fig. 3b) (Supplementary Table 1; Model 1). However, neither low- nor high-frequency strain led to an increase in percent 3-NT positive intimal lining CD68 + macrophages (Supplementary Table 1; Model 2). Interestingly, when controlling for the interaction between CD68 + macrophage content in the synovial intima and tensile strain frequency, the total %3-NT positive intimal lining cells increased even further (26.29 [95%CI 6.68, 45.89]) (Supplementary Table 1; Model 3).

Discussion

The synovium is critical for maintaining joint health^{3,4} and synovial pathology (especially synovitis) is associated with pain and disease progression in OA. Characterizing synovial tissue responses to mechanical loading is therefore critical to understand the biological effects of physical activity, which is often associated with joint swelling and painful experiences for patients with knee OA. We found that intact synovial tissue demonstrated frequency-dependent responses to tensile strain at frequencies similar to slow (~ 40 cycles per minute) or faster (~ 120 cycles per minute) flexion–extension joint movement cycles. In particular, we observed changes in cell metabolism, oxidative stress, and inflammatory signaling.

Low-frequency tensile strain was better tolerated by OA synovium and led to enrichment in processes such as interferon-gamma and -alpha responses, Fc receptor signaling pathways, and lysosomal routing. Each of these processes are critical for recruitment of cells involved in immune regulation and resolution of innate immune responses^{25,31,32}, suggesting that low-frequency strain may stimulate inflammation resolution mechanisms. This was further supported by decreased expression of *SERPIN* genes and the nuclear repressor of *CLOCK* (*PASD1*³³).

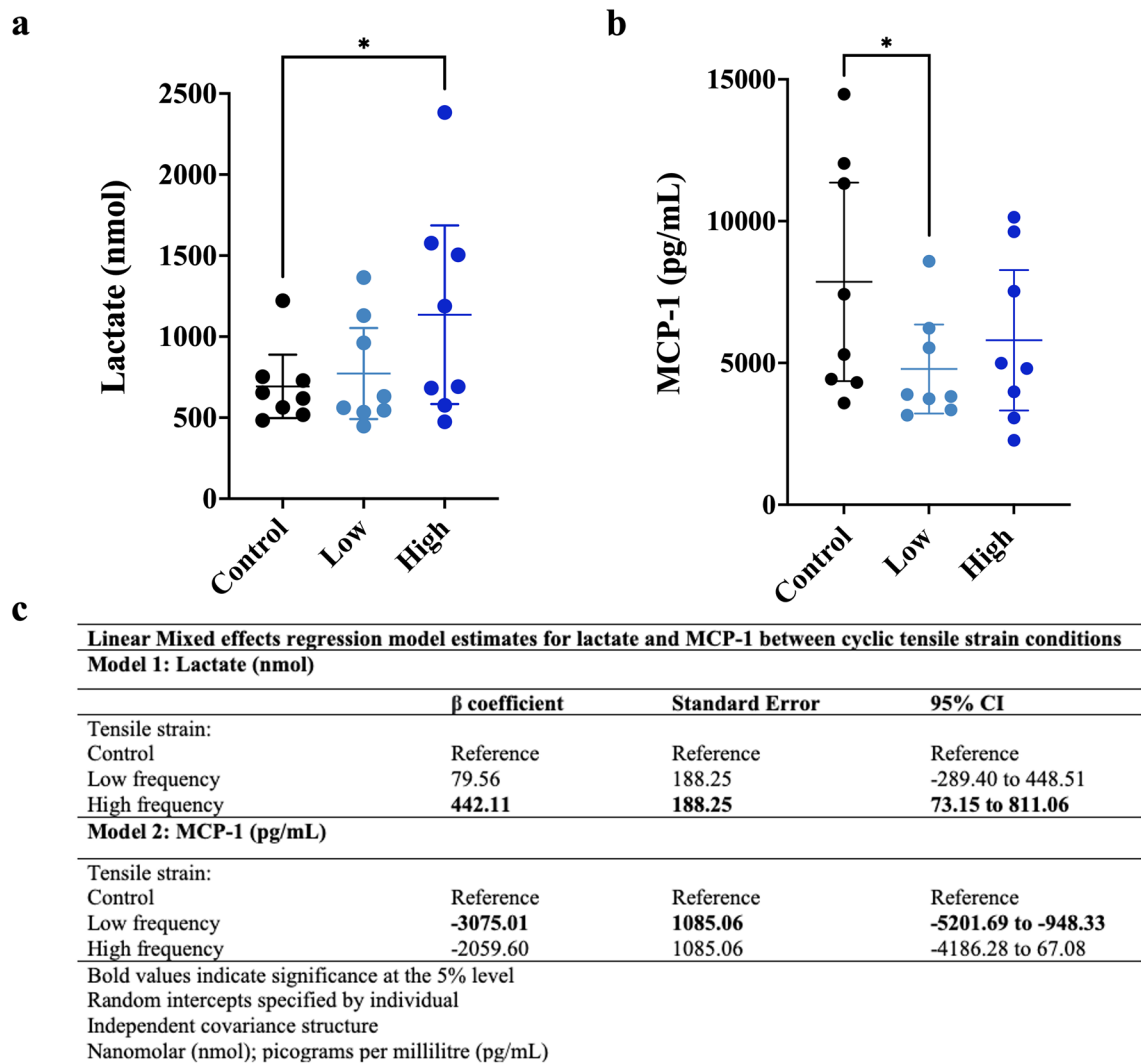


Figure 2. Lactate and MCP-1 release into conditioned media from synovial tissue. **(a)** Dot plot displaying the individual lactate measures as well as the mean \pm 95% CI of lactate for Control (black), Low (light blue), and High (dark blue) strain conditions. **(b)** Dot plot displaying the individual MCP-1 measures as well as the mean \pm 95% CI of lactate for Control (black), Low (light blue), and High (dark blue) strain conditions. **(c)** Linear mixed effects model estimates for lactate (Model 1) and MCP-1 (Model 2) in conditioned media for each cyclic tensile strain condition. CI, confidence interval; nmol, nanomolar; pg/mL, picogram per millilitre.

SERPINs increase during inflammation to mitigate the damaging effects of uncontrolled enzyme activity and then decrease as inflammation resolves³⁴. Similarly, *CLOCK* repressors inhibit the ability to maintain cell metabolism, homeostasis, and circadian rhythm^{35,36}. Low-frequency tensile strain also led to enrichment of metabolism and cell stress pathways without inducing increases in lactate release or 3-NT formation, and reduced MCP-1 release compared to control. In contrast, high-frequency strain increased lactate release and 3-NT formation, abrogated the reduction in MCP-1 release, and stimulated greater enrichment of more harmful immune signaling processes such as NOD-like receptor signaling and neutrophil degranulation, suggesting a physiologic shift toward pro-inflammatory signaling pathways^{37–39}. Similarly, glyoxylate metabolism was enriched, suggesting increases in ER stress and/or accumulation of glyoxylate in the cytoplasm causing cell damage⁴⁰.

These whole-tissue findings are conceptually similar to an *in vitro* monolayer study by Takao et al.¹⁹, where tensile strain increased expression of pro-inflammatory genes (*COX2*, *IL-1 β*) and synthesis of PGE2 in human synovial fibroblasts. In that study, overexpression of hemeoxygenase-1 suppressed pro-inflammatory responses in fibroblasts, suggesting that the pro-inflammatory responses were due to mechanical induction of cellular oxidative stress¹⁹. Inflammation and oxidative stress are known to inhibit and damage mitochondria⁴¹, increasing levels of nitric oxide and superoxide and thus the formation of 3-NT. Our results therefore collectively suggest that the limits of OA synovial tissues to tolerate tensile strain forces were exceeded at high-frequency, but not low-frequency strain, and for context low-frequency and high-frequency flexion–extension joint movements may be similar to slow and faster walking speeds, respectively. Indeed, it is well-established that exercise and physical activity are beneficial for synovial joints, particularly in the medium to longer term^{42,43}. However, patients with late-stage knee OA typically demonstrate acute, symptomatic intolerance to fast-paced walking, which aligns with

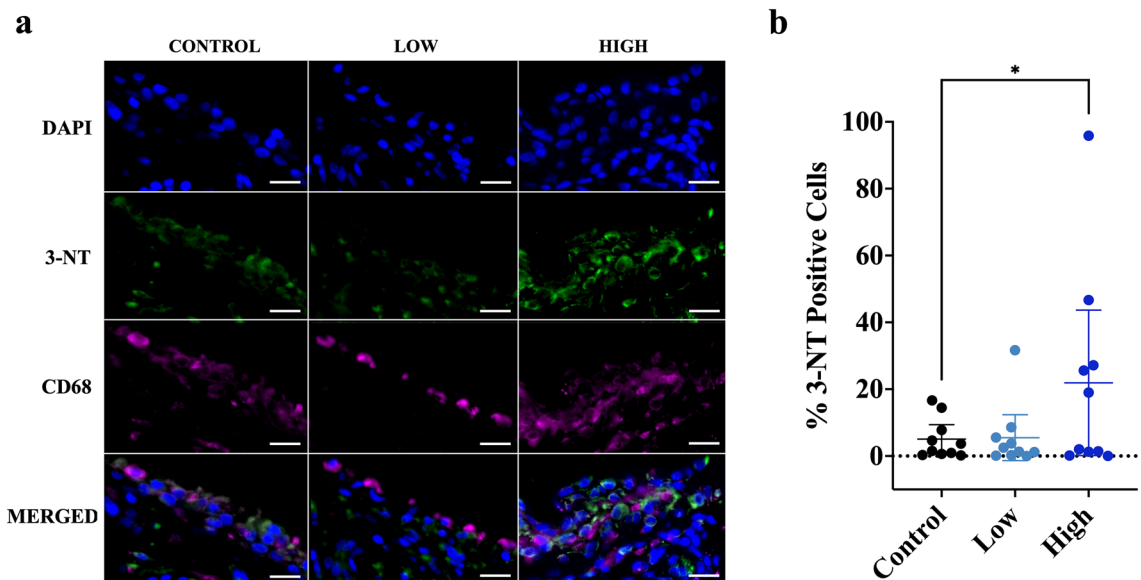


Figure 3. Cyclic tensile strain increases 3-NT staining in OA synovial tissue. **(a)** Representative immunofluorescence images of 3-NT (green) and CD68 (magenta) for each cyclic tensile strain loading condition. **(b)** Dot plots displaying the individual 3-NT+ cells (mean \pm 95% CI) for Control (black), Low (light blue), and High (dark blue) tensile strain conditions. Scale bar = 20 μ m. 3-NT, 3-Nitrotyrosine; CD68, macrophage marker; CI, confidence interval; DAPI, nuclear stain.

our *ex vivo* observations in synovial tissue demonstrating that high-frequency tensile strain provokes cell stress responses in the short-term. Since we expect that these frequencies would be well-tolerated in healthy tissues, our findings suggest that OA may cause derangements in synovial tissue physiology and thereby lower tolerance to mechanical loads. This concept has been shown in the temporomandibular joint, where overloading shifts the homeostatic balance of anabolic and catabolic processes^{44,45}. Such physiologic impairments may potentially have clinically relevant implications such as longer recovery times and/or poor joint and patient outcomes.

Our data provide some clues to how OA may lower tolerance to mechanical loading, resulting in inflammatory signaling and oxidative stress responses. High-frequency tensile strain led to higher energy demand with enrichment of glyoxylate metabolism and glycine catabolism, cytochrome metabolism, and ER stress pathways. These changes were driven in part by increased expression of genes responsible for handling excess metabolite build up and cell stress including *CYP*, *UGT*, and *FDX*^{26–28}. Thus, OA may reduce the ability to process the buildup of excess metabolites during high energy demand, which would lead to ROS generation. Since synovial lining macrophages play important roles in OA inflammation and are an important source of reactive oxygen species (ROS) generation⁴⁶, we were surprised that 3-NT staining was not increased in lining macrophages by tensile loading. Instead, higher proportions of synovial lining macrophages were associated with greater 3-NT staining in lining cells overall when we controlled for interactions between macrophage content and tensile strain frequency in our models. This suggests macrophages influence mechanobiological responses to tensile strain loading through nitric oxide signaling. Prior studies have also demonstrated that macrophages can modulate the redox metabolism of their resident tissue. A study by Wu et al. (2013) reported that cyclic strain activated the inflammasome as a result of mitochondrial ROS in tissue-resident macrophages in the lung, which contributed to mechanical ventilation injury⁴⁷. Considering our results, this concept should be investigated further in the context of OA. Additionally, since our findings are at the level of the whole tissue, future studies should consider single-cell RNA sequencing or spatial profiling to tease out the specific cell populations that may be responsible for the mechanobiological responses of the synovium.

Limitations of our study include the testing of synovial tissue samples only from late-stage OA patients undergoing joint replacement surgery, which may have responded differently from synovium from earlier stages of knee OA or healthy joints without OA. Future studies should attempt to include synovial biopsy samples from non-OA comparator tissues; however, access to these tissues in the quantity required for this type of experiment is often limited. Prior literature suggests that the forces experienced by synovial tissue in the mechanical stimulation protocol applied include both tensile strain and convective forces^{1,2}, which should be considered when interpreting our findings. Mechanical stimulation occurred in atmospheric oxygen (considered hyperoxic compared to adapted cells in the body) and this may play a role in modulating some metabolic features of the response to tensile strain. We focused our measurements at 6-h post-strain to assess early transcriptomic changes in response to loading, but different physiologic responses may occur immediately or much later after loading and should be explored in future studies. Patient confounders such as age, sex, BMI, and inflammatory status of the tissue may influence responses to cyclic tensile strain. We attempted to match patients by covariates, but these factors likely led to some degree of noise in our data, potentially precluding the detection of smaller physiologic responses to cyclic tensile strain.

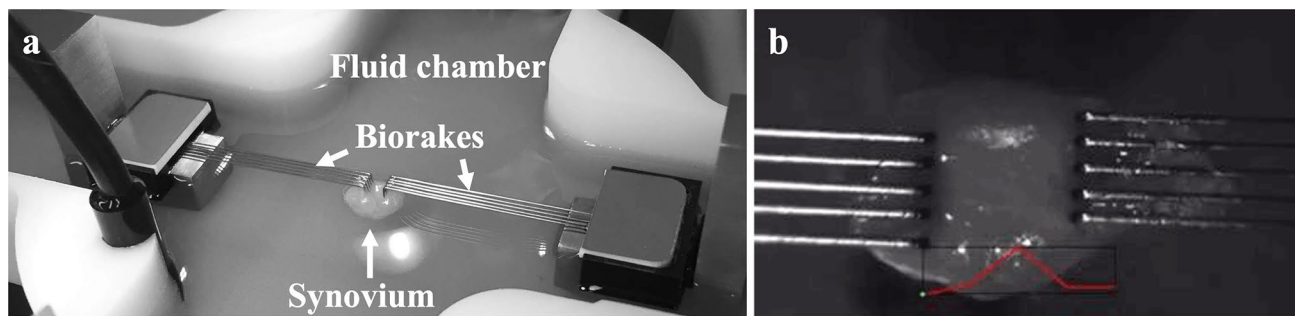


Figure 4. Synovial cyclic tensile strain experimental set up. (a) Representative image of synovial tissue sample loaded on CellScale BioTester apparatus. (b) Close up image of synovial tissue attached to Biorakes with strain displacement graph (red).

Patients with OA experience increased pain or joint swelling during physical activity, which may in part be related to the mechanobiological responses of the synovium. To our knowledge, this is the first study to report transcriptomic and supporting physiologic data describing responses to tensile strain loading in whole synovial tissues from patients with knee OA. Given the strength of oxidative stress responses observed, we speculate that late-stage knee OA renders the synovium susceptible to oxidative stress as a result of high frequency strain loading. Formation of 3NT implies the presence of high concentrations of nitric oxide and superoxide under strain conditions. Localization of these signals to the synovial lining and not macrophages themselves suggests that macrophages may be excreting nitric oxide that then interacts with intracellular superoxide in other synovial cell types; however, this needs to be investigated further. Physiologic responses to tensile loading in late-stage OA synovium include increased inflammatory signaling mechanisms, shifts in cell metabolism, and redox-related cell stress, which appear to be frequency-dependent. These findings represent candidate mechanisms that may be relevant to activity-related joint outcomes and provide a useful experimental model for further investigation.

Methods

Study participants and synovial tissue biopsies. Synovial tissue samples were collected from 10 sequential participants undergoing total knee arthroplasty (TKA) between January 2019 and July 2019. All included study participants had symptomatic, late-stage knee OA, with severe radiographic damage (Kellgren-Lawrence (KL) grade 3 or 4) warranting TKA. Patients provided written informed consent and the study was approved by Western University's Research Ethics Board for Health Sciences Research Involving Human Patients (HSREB #109255) and this research was performed in accordance with the Declaration of Helsinki. During TKA, synovial biopsies were acquired from a standardized location in the lateral suprapatellar recess. An 8 mm diameter biopsy punch was used to collect standardized, adjacent biopsies of glassy-appearing synovial membrane, providing a set of 4 equal-sized pieces of tissue with a similar gross appearance from each patient. One piece of tissue was processed for routine histopathology with the remaining 3 pieces allocated to mechanical loading experiments.

Cyclic tensile strain protocol. A CellScale BioTester (CellScale, Waterloo, Canada) was used to apply controlled cyclic uniaxial strain to synovial tissue to model the tensile forces experienced by synovial tissues during rest and slow or fast flexion–extension joint movements. The tissue was secured to the BioTester using tissue Biorakes (tine diameter = 254 μm ; tine spacing = 0.7 mm; puncture depth = 2.0 mm) and a 0.5 Newton (N) load cell was used for experimental tensile strain protocol. The fluid chamber was filled with DMEM and maintained at 37 $^{\circ}\text{C}$ (Fig. 4). Since there have been no previous studies assessing mechanical strain in whole synovium, limits testing was completed by loading pilot tissue samples at 10%, 20%, 30%, and 40% strain while monitoring force readouts for failure of the tissue (sudden drop in force), which occurred at 30% strain or higher. Ten percent strain was selected to apply gentle loading and avoid tissue failure and has been used previously in the literature for mechanical stimulation of cell monolayers¹⁹. Three matched pieces of synovial tissue per patient underwent one of 3 tensile strain (10%) loading protocols for 30 min each: (1) low-frequency cyclic tensile strain (0.3 Hz—40 cycles/min), (2) high-frequency cyclic tensile strain (1.0 Hz—120 cycles/min), or (3) static control (tissues mounted on Biorakes and held for 30 min at 20 mN preload required to remain attached). Following each loading protocol, each tissue piece was placed in one well of a 12-well plate containing 1.0 mL of fresh serum-free DMEM, and incubated at 37 $^{\circ}\text{C}$, 5% CO_2 for 6 h. The conditioned media was then collected and placed in short-term cryostorage for downstream assays.

Tissue homogenization and RNA purification. Synovial tissues were bisected; one half was homogenized in 1 mL of Trizol and stored at -20-degrees until RNA purification. The Direct-zolTM RNA Microprep RNA purification kit (Zymo Research, Irvine, USA) was used to purify whole tissue RNA. The other half of the tissue was processed for paraffin embedding, histopathology, and immunostaining (see below).

RNA library preparation and sequencing. Total RNA was quantified using the NanoDrop (Thermo Fisher Scientific, Waltham, MA), RNA quality was assessed using the Agilent 2100 Bioanalyzer (Agilent Tech-

nologies Inc., Palo Alto, CA) and the RNA 6000 Nano kit (Caliper Life Sciences, Mountain View, CA). Synovial tissue RNA samples were included for RNA sequencing analysis if all 3 samples from an individual patient met the RNA quality (RIN > 8.0) and quantity requirements. RNA sequencing was performed at the London Regional Genomics Centre (Robarts Research Institute, London, Canada). The TruSeq Stranded Total RNA Library Prep Gold kit (Illumina, San Diego, CA, USA) was used. Samples were rRNA depleted, fragmented, cDNA was synthesized, indexed, cleaned-up and amplified via PCR. Libraries were pooled in equimolar ratio into one library. Size distribution was assessed on an Agilent High Sensitivity DNA Bioanalyzer chip and quantitated using the Qubit 2.0 Fluorimeter (Thermo Fisher Scientific, Waltham, MA). The library was sequenced on an Illumina NextSeq 500 as 2 × 76 bp paired end runs, using one High Output v2 kit (150 cycles).

Analysis of RNA-sequencing data. Raw FASTA files (runs and lanes) were concatenated to form the final FASTQ files to be used in the rest of the pipeline. R code was developed and run in RStudio (Version: 1.2.5001)⁴⁸. fastp (version 0.20.0) was used to collect QC metrics of the raw reads⁴⁹. RNA sequences were aligned and sorted by coordinates, to the NCBI human genome build 38 version 98, using STAR aligner (STAR-2.7.2c)⁵⁰. The removal of alignment duplicates was done with Sambamba (version 0.7.0)⁵¹. Quantification of genes was performed using featureCounts (v1.6.3)⁵². DESeq2 (v 1.24.0)^{53,54} was used to normalize feature counts and to find the differentially expressed genes. The HGNC symbols were extracted and added to the DESeq2 results data frame using biomaRt (version 2.40.4)^{55,56} using the "hsapiens_gene_ensembl" dataset and the "Ensembl Release 98 (September 2019)" mart. Significantly differentially expressed genes were identified using the following criteria: p-value < 0.05 (corresponds to a $-\log_{10}[p\text{-value}] > 1.3$) and a log₂ fold change > ± 1.0 (corresponds to an absolute fold change of 2.0). Volcano plots of differentially expressed genes were created using GraphPad Prism (version 9.0) software (San Diego CA, USA) with these criteria. Gene ontology (<http://geneontology.org/>) was used to determine pathway enrichment of the differentially expressed genes for each tensile strain condition: low-frequency versus control and high-frequency versus control. Venny 2.1.0⁵⁷ was used to compare/contrast differentially expressed genes. Gene Set Enrichment Analysis (GSEA version 4.1.0)^{58,59} of normalized gene counts was used to identify significantly enriched gene sets/pathways by each tensile strain condition using the Hallmark and Reactome collections from the Molecular Signatures Database (MSigDB) as follows: low-frequency versus control, high-frequency versus control, and high-frequency versus low-frequency tensile strain. The Hallmark gene sets include 50 well-defined biological states or processes and the Reactome gene sets include over 1000 gene sets related to biological signaling, transcriptional regulation, and metabolism. Significant enrichment was determined by a false discovery rate (FDR) cut-off value of < 0.05. Leading edge analysis was completed in GSEA (version 4.1.0) to identify the top genes that contribute to the enrichment of multiple Reactome gene sets related to cell stress and cell metabolism.

L(+)-lactate assay of conditioned media samples. A fluorometric assay kit (Biovision, Mountain View, CA, USA) was used to measure L(+)-lactate release in conditioned media samples in duplicate using a microplate reader with excitation at 535 nm and emission at 590 nm. Amount (nanomolar; nmol) of lactate present in each sample was interpolated using the standard curve. Linear mixed effects regression models were used to assess differences in lactate between tensile strain loading conditions (control, low, and high), while adjusting for differences between patients (random intercepts). Results were reported as unstandardized beta (β) coefficients with 95% CIs and standard errors.

Enzyme-linked immunosorbent assay of MCP-1 in conditioned media samples. A LEGEND MAX™ assay kit (BioLegend, San Diego, CA, USA) was used to measure monocyte chemoattractant protein-1 (MCP-1) in conditioned media samples in duplicate. Absorbance at 570 nm was subtracted from the absorbance reading at 450 nm. Amount (picogram per millilitre; pg/mL) of MCP-1 present in each sample was interpolated using the standard curve. Linear mixed effects regression models were used to assess differences in MCP-1 between tensile strain loading conditions (control, low, and high), while adjusting for differences between patients (random intercepts). Results were reported as unstandardized beta (β) coefficients with 95% CIs and standard errors.

Synovial tissue histopathology. Synovial tissue was fixed in 4% paraformaldehyde and paraffin embedded. Tissue samples were sectioned on a microtome at 5 μm thickness, stained with hematoxylin and eosin and scored using 5 non-overlapping, high-power fields (hpf, 400X) per patient. Six histopathological components were graded on a 0–3 scale (normal to severe) as previously described⁶⁰. Mean and median scores for each component were calculated using the average or median score across 5 sections.

Synovial tissue immunofluorescence. Synovial tissues sections were deparaffinized and antigen retrieval was performed in sodium citrate buffer (10 mM sodium citrate, 0.05% Tween-20, pH 6) at 55 °C overnight. Slides were permeabilized with Triton-X (0.2% in PBS; Sigma-Aldrich; 9002-93-1) and blocked for 1 h with 5% bovine serum albumin (BSA; GE Healthcare). Samples were incubated with primary antibodies overnight at 4 °C for anti-CD68 (Abcam, 1:200) in combination with anti-3-NT (Abcam, 1:150). Negative control sections without primary antibody were included to rule out non-specific secondary antibody binding. Slides were incubated with appropriate secondary antibodies including goat anti-mouse conjugated with Alexa Fluor-647 (Jackson ImmunoResearch Laboratories: 1:500) or goat anti-rabbit conjugated with Alexa Fluor-488 (Jackson ImmunoResearch Laboratories: 1:500). Coverslips were mounted using Molecular Probes ProLong Gold Antifade Mountant containing DAPI nuclear stain (Fisher Scientific, P36931). Slides were imaged at 40X using a Leica Aperio VERSA 8 microscopic scanner located at Molecular Pathology Core Facility, Robart's Research

Institute. Images were analyzed using QuPath (v0.2.3) cell detection and classifier tools⁶¹. We assessed 3-NT positive cells in the synovial intimal lining (normalized to cell density). We also assessed 3-NT staining relative to cell type content (i.e., CD68+ (macrophage) vs CD68- cells in the synovial lining). Linear mixed effects regression was used to investigate (1) the association between percent positive 3-NT cells and tensile strain condition, while controlling for variation between patient samples (random intercepts) and (2) the association between 3-NT positive macrophages and tensile strain condition. Secondary analyses included (1) controlling for total synovial lining macrophage content and (2) including a strain by macrophage content interaction term. Results are reported as unstandardized beta coefficients (β) with 95% confidence intervals (CI).

Data availability

The RNA sequencing datasets generated and analyzed during the current study are available at Gene Expression Omnibus (GEO) repository, accession number: GSE205196. All other data is available upon reasonable request.

Received: 25 May 2022; Accepted: 14 October 2022

Published online: 17 October 2022

References

- McCarty, W. J., Masuda, K. & Sah, R. L. Fluid movement and joint capsule strains due to flexion in rabbit knees. *J. Biomech.* **44**, 2761–2767. <https://doi.org/10.1016/j.jbiomech.2011.09.005> (2011).
- Ingram, K. R., Wann, A. K. T., Angel, C. K., Coleman, P. J. & Levick, J. R. Cyclic movement stimulates hyaluronan secretion into the synovial cavity of rabbit joints. *J. Physiol.* **586**, 1715–1729. <https://doi.org/10.1113/jphysiol.2007.146753> (2008).
- Mathiessen, A. & Conaghan, P. G. Synovitis in osteoarthritis: Current understanding with therapeutic implications. *Arthritis Res. Ther.* **19**, 18. <https://doi.org/10.1186/s13075-017-1229-9> (2017).
- Robinson, W. H. *et al.* Low-grade inflammation as a key mediator of the pathogenesis of osteoarthritis. *Nat. Rev. Rheumatol.* **12**, 580–592. <https://doi.org/10.1038/nrrheum.2016.136> (2016).
- Guermazi, A. *et al.* Synovitis in Knee Osteoarthritis Assessed by contrast-enhanced magnetic resonance imaging (MRI) is associated with radiographic tibiofemoral osteoarthritis and MRI-detected widespread cartilage damage: The MOST study. *J. Rheumatol.* **41**, 501–508. <https://doi.org/10.3899/jrheum.130541> (2014).
- Hill, C. L. *et al.* Synovitis detected on magnetic resonance imaging and its relation to pain and cartilage loss in knee osteoarthritis. *Ann. Rheum. Dis.* **66**, 1599. <https://doi.org/10.1136/ard.2006.067470> (2007).
- Baker, K. *et al.* Relation of synovitis to knee pain using contrast-enhanced MRIs. *Ann. Rheum. Dis.* **69**, 1779. <https://doi.org/10.1136/ard.2009.121426> (2010).
- Oo, W. M. *et al.* Are OMERACT knee osteoarthritis ultrasound scores associated with pain severity, other symptoms, and radiographic and magnetic resonance imaging findings? *J. Rheumatol.* **48**, 270–278. <https://doi.org/10.3899/jrheum.191291> (2020).
- Conaghan, P. G. *et al.* Clinical and ultrasonographic predictors of joint replacement for knee osteoarthritis: Results from a large, 3-year, prospective EULAR study. *Ann. Rheum. Dis.* **69**, 644. <https://doi.org/10.1136/ard.2008.099564> (2010).
- Nielsen, F. K., Egdand, N., Jørgensen, A. & Jurik, A. G. Risk factors for joint replacement in knee osteoarthritis; a 15-year follow-up study. *BMC Musculoskelet. Disord.* **18**, 510. <https://doi.org/10.1186/s12891-017-1871-z> (2017).
- Coleman, M. C. *et al.* Targeting mitochondrial responses to intra-articular fracture to prevent posttraumatic osteoarthritis. *Sci. Transl. Med.* **10**, eaan5372. <https://doi.org/10.1126/scitranslmed.aan5372> (2018).
- Chou, C.-H. *et al.* Synovial cell cross-talk with cartilage plays a major role in the pathogenesis of osteoarthritis. *Sci. Rep.-UK* **10**, 10868. <https://doi.org/10.1038/s41598-020-67730-y> (2020).
- Hunter, D. J. & Eckstein, F. Exercise and osteoarthritis. *J. Anatomy* **214**, 197–207. <https://doi.org/10.1111/j.1469-7580.2008.01013.x> (2009).
- Ernstgård, A., PirouziFard, M. & Thorstensson, C. A. Health enhancing physical activity in patients with hip or knee osteoarthritis—an observational intervention study. *BMC Musculoskelet. Disord.* **18**, 42. <https://doi.org/10.1186/s12891-017-1394-7> (2017).
- Focht, B. C., Ewing, V., Gauvin, L. & Rejeski, W. J. The unique and transient impact of acute exercise on pain perception in older, overweight, or obese adults with knee osteoarthritis. *Ann. Behav. Med.* **24**, 201–210. https://doi.org/10.1207/s15324796abm2403_05 (2002).
- Peeva, E. *et al.* A walking model to assess the onset of analgesia in osteoarthritis knee pain. *Osteoarthr. Cartilage* **18**, 646–653. <https://doi.org/10.1016/j.joca.2009.12.008> (2010).
- Sandal, L. F., Roos, E. M., Bøgesvang, S. J. & Thorlund, J. B. Pain trajectory and exercise-induced pain flares during 8 weeks of neuromuscular exercise in individuals with knee and hip pain. *Osteoarthr. Cartilage* **24**, 589–592. <https://doi.org/10.1016/j.joca.2015.11.002> (2016).
- Rohanifar, M. *et al.* Hydraulic permeability and compressive properties of porcine and human synovium. *Biophys. J.* <https://doi.org/10.1016/j.bpj.2022.01.008> (2022).
- Takao, M. *et al.* Role of heme oxygenase-1 in inflammatory response induced by mechanical stretch in synovial cells. *Inflamm. Res.* **60**, 861–867. <https://doi.org/10.1007/s00011-011-0346-1> (2011).
- Schröder, A. *et al.* Impact of mechanical load on the expression profile of synovial fibroblasts from patients with and without osteoarthritis. *Int. J. Mol. Sci.* **20**, 585. <https://doi.org/10.3390/ijms20030585> (2019).
- Sambajon, V. V., Cillo, J. E., Gassner, R. J. & Buckley, M. J. The effects of mechanical strain on synovial fibroblasts. *J. Oral Maxil. Surg.* **61**, 707–712. <https://doi.org/10.1053/joms.2003.50141> (2003).
- Nazet, U. *et al.* Differential gene expression response of synovial fibroblasts from temporomandibular joints and knee joints to dynamic tensile stress. *J. Orofac. Orthop. Fortschritte Der Kieferorthopädie* **2021**, 1–15. <https://doi.org/10.1007/s00056-021-00309-y> (2021).
- Benito, M. J., Veale, D. J., FitzGerald, O., Berg, W. B. V. D. & Bresnihan, B. Synovial tissue inflammation in early and late osteoarthritis. *Ann. Rheum. Dis.* **64**, 1263. <https://doi.org/10.1136/ard.2004.025270> (2005).
- Wood, M. J. *et al.* Macrophage proliferation distinguishes 2 subgroups of knee osteoarthritis patients. *JCI Insight* **4**, e125325. <https://doi.org/10.1172/jci.insight.125325> (2019).
- Timur, Z. K., Demir, S. A. & Seyrantepe, V. Lysosomal cathepsin A plays a significant role in the processing of endogenous bioactive peptides. *Front. Mol. Biosci.* **3**, 68. <https://doi.org/10.3389/fmolb.2016.00068> (2016).
- Nebert, D. W., Wikvall, K. & Miller, W. L. Human cytochromes P450 in health and disease. *Philos. Trans. R. Soc. B Biol. Sci.* **368**, 20120431. <https://doi.org/10.1098/rstb.2012.0431> (2013).
- Sheftel, A. D. *et al.* Humans possess two mitochondrial ferredoxins, Fdx1 and Fdx2, with distinct roles in steroidogenesis, heme, and Fe/S cluster biosynthesis. *Proc. Natl. Acad. Sci.* **107**, 11775–11780. <https://doi.org/10.1073/pnas.1004250107> (2010).

28. Kalthoff, S., Ehmer, U., Freiberg, N., Manns, M. P. & Strassburg, C. P. Interaction between oxidative stress sensor Nrf2 and xenobiotic-activated aryl hydrocarbon receptor in the regulation of the human phase II detoxifying UDP-glucuronosyltransferase 1A10*. *J. Biol. Chem.* **285**, 5993–6002. <https://doi.org/10.1074/jbc.m109.075770> (2010).
29. Pickart, C. M. Mechanisms underlying ubiquitination. *Biochemistry-US* **70**, 503–533. <https://doi.org/10.1146/annurev.biochem.70.1.503> (2001).
30. Hochstrasser, M. Ubiquitin, proteasomes, and the regulation of intracellular protein degradation. *Curr. Opin. Cell Biol.* **7**, 215–223. [https://doi.org/10.1016/0955-0674\(95\)80031-x](https://doi.org/10.1016/0955-0674(95)80031-x) (1995).
31. Takai, T. Fc receptors and their role in immune regulation and autoimmunity. *J. Clin. Immunol.* **25**, 1–18. <https://doi.org/10.1007/s10875-005-0353-8> (2005).
32. Lee, A. J. & Ashkar, A. A. The dual nature of type I and type II interferons. *Front. Immunol.* **9**, 2061. <https://doi.org/10.3389/fimmu.2018.02061> (2018).
33. Michael, A. K. *et al.* Cancer/testis antigen PASD1 silences the circadian clock. *Mol. Cell* **58**, 743–754. <https://doi.org/10.1016/j.molcel.2015.03.031> (2015).
34. Bao, J. *et al.* Serpin functions in host-pathogen interactions. *PeerJ* **6**, e4557. <https://doi.org/10.7717/peerj.4557> (2018).
35. Dibner, C., Schibler, U. & Albrecht, U. The Mammalian circadian timing system: Organization and coordination of central and peripheral clocks. *Annu. Rev. Physiol.* **72**, 517–549. <https://doi.org/10.1146/annurev-physiol-021909-135821> (2010).
36. Gachon, F., Nagoshi, E., Brown, S. A., Ripperger, J. & Schibler, U. The mammalian circadian timing system: From gene expression to physiology. *Chromosoma* **113**, 103–112. <https://doi.org/10.1007/s00412-004-0296-2> (2004).
37. Wen, H., Miao, E. A. & Ting, J. P. Y. Mechanisms of NOD-like receptor-associated inflammasome activation. *Immunity* **39**, 432–441. <https://doi.org/10.1016/j.immuni.2013.08.037> (2013).
38. Schroder, K., Kanneganti, T.-D., Shao, F. & Broz, P. Mechanisms and consequences of inflammasome activation. *J. Mol. Biol.* **430**, 131–132. <https://doi.org/10.1016/j.jmb.2017.12.005> (2018).
39. Wright, H. L., Moots, R. J. & Edwards, S. W. The multifactorial role of neutrophils in rheumatoid arthritis. *Nat. Rev. Rheumatol.* **10**, 593–601. <https://doi.org/10.1038/nrrheum.2014.80> (2014).
40. Laido, E., Pey, A. L., Rodriguez, R. & Lorenzo, V. Primary hyperoxalurias: Disorders of glyoxylate detoxification. *Biochim. Biophys. Acta BBA Mol. Basis Dis.* **1822**, 1453–1464. <https://doi.org/10.1016/j.bbadis.2012.03.004> (2012).
41. Chen, Y., Zhou, Z. & Min, W. Mitochondria, oxidative stress and innate immunity. *Front. Physiol.* **9**, 1487. <https://doi.org/10.3389/fphys.2018.01487> (2018).
42. Driban, J. B., Hootman, J. M., Sitler, M. R., Harris, K. & Cattano, N. M. Is participation in certain sports associated with knee osteoarthritis? A systematic review. *J. Athl. Train.* **52**, 497–506. <https://doi.org/10.4085/1062-6050-50.2.08> (2015).
43. Lefèvre-Colau, M.-M. *et al.* Is physical activity, practiced as recommended for health benefit, a risk factor for osteoarthritis?. *Ann. Phys. Rehabil. Med.* **59**, 196–206. <https://doi.org/10.1016/j.rehab.2016.02.007> (2016).
44. Asakawa-Tanne, Y. *et al.* Effects of enzymatic degradation after loading in temporomandibular joint. *J. Dent. Res.* **94**, 337–343. <https://doi.org/10.1177/0022034514560588> (2015).
45. Tanaka, E. & Koolstra, J. H. Biomechanics of the temporomandibular joint. *J. Dent. Res.* **87**, 989–991. <https://doi.org/10.1177/154405910808701101> (2008).
46. Ryan, D. G. & O'Neill, L. A. J. Krebs cycle reborn in macrophage immunometabolism. *Annu. Rev. Immunol.* **38**, 1–25. <https://doi.org/10.1146/annurev-immunol-081619-104850> (2020).
47. Wu, J. *et al.* Activation of NLRP3 inflammasome in alveolar macrophages contributes to mechanical stretch-induced lung inflammation and injury. *J. Immunol.* **190**, 3590–3599. <https://doi.org/10.4049/jimmunol.1200860> (2013).
48. Team, R. *RStudio: Integrated Development for R*. <http://www.rstudio.com/> (2020).
49. Chen, S., Zhou, Y., Chen, Y. & Gu, J. fastp: An ultra-fast all-in-one FASTQ preprocessor. *Bioinformatics* **34**, i884–i890. <https://doi.org/10.1093/bioinformatics/bty560> (2018).
50. Dobin, A. *et al.* STAR: Ultrafast universal RNA-seq aligner. *Bioinformatics* **29**, 15–21. <https://doi.org/10.1093/bioinformatics/bts635> (2013).
51. Tarasov, A., Vilella, A. J., Cuppen, E., Nijman, I. J. & Prins, P. Sambamba: Fast processing of NGS alignment formats. *Bioinformatics* **31**, 2032–2034. <https://doi.org/10.1093/bioinformatics/btv098> (2015).
52. Liao, Y., Smyth, G. K. & Shi, W. featureCounts: An efficient general purpose program for assigning sequence reads to genomic features. *Bioinformatics* **30**, 923–930. <https://doi.org/10.1093/bioinformatics/btt656> (2014).
53. Love, M. I., Huber, W. & Anders, S. Moderated estimation of fold change and dispersion for RNA-seq data with DESeq2. *Genome Biol.* **15**, 550. <https://doi.org/10.1186/s13059-014-0550-8> (2014).
54. Team, R. C. R: *A language and environment for statistical computing*. <https://www.R-project.org/> (2018).
55. Durinck, S. *et al.* BioMart and Bioconductor: A powerful link between biological databases and microarray data analysis. *Bioinformatics* **21**, 3439–3440. <https://doi.org/10.1093/bioinformatics/bti525> (2005).
56. Durinck, S., Spellman, P. T., Birney, E. & Huber, W. Mapping identifiers for the integration of genomic datasets with the R/Bioconductor package biomaRt. *Nat. Protoc.* **4**, 1184–1191. <https://doi.org/10.1038/nprot.2009.97> (2009).
57. Oliveros, J. *VENNY. An Interaction Tool for Comparing Lists with Venn Diagrams* <https://bioinfogp.cnb.csic.es/tools/venny/> (2022).
58. Subramanian, A. *et al.* Gene set enrichment analysis: A knowledge-based approach for interpreting genome-wide expression profiles. *Proc. Natl. Acad. Sci. USA* **102**, 15545–15550. <https://doi.org/10.1073/pnas.0506580102> (2005).
59. Mootha, V. K. *et al.* PGC-1 α -responsive genes involved in oxidative phosphorylation are coordinately downregulated in human diabetes. *Nat. Genet.* **34**, 267–273. <https://doi.org/10.1038/ng1180> (2003).
60. Minten, M. J. M. *et al.* Exploring longitudinal associations of histologically assessed inflammation with symptoms and radiographic damage in knee osteoarthritis: Combined results of three prospective cohort studies. *Osteoarthritis Cartilage* **27**, 71–79. <https://doi.org/10.1016/j.joca.2018.10.014> (2018).
61. Bankhead, P. *et al.* QuPath: Open source software for digital pathology image analysis. *Sci. Rep.-UK* **7**, 16878. <https://doi.org/10.1038/s41598-017-17204-5> (2017).

Acknowledgements

The authors would like to acknowledge all members of the WOREO Knee Study team, especially Drs. Brent A. Lanting, Steven J. MacDonald, and Edward M. Vasarhelyi for access to synovial tissues. We would like to thank David Carter of the London Regional Genomics Centre (Robart's Research Institute, London, ON, Canada) for library preparation and RNA sequencing, Hao Yin of the Molecular Pathology Core Facility (Robart's Research Institute) for scanning our immunofluorescence slides, and Dale Fournier for his assistance with developing the BioTester cyclic tensile strain protocol.

Author contributions

HTP contributed to the study conception and design, data acquisition, data analysis/interpretation, and drafted manuscript. BF completed pre-processing of RNA sequencing data, completed differential gene expression

analysis, and revised manuscript. TBB, LAW, MCC, CAS, CTA contributed to the study conception and design, data interpretation, and edited manuscript. All authors critically reviewed and approved the manuscript.

Funding

This work was funded in part by grants from the Academic Medical Organization of Southwestern Ontario (AMOSO), the Canada Research Chairs program, and Western University's Bone and Joint Institute. HTP is supported by Frederick Banting and Charles Best Doctoral Award from CIHR.

Competing interests

The authors declare no competing interests.

Additional information

Supplementary Information The online version contains supplementary material available at <https://doi.org/10.1038/s41598-022-22459-8>.

Correspondence and requests for materials should be addressed to C.T.A.

Reprints and permissions information is available at www.nature.com/reprints.

Publisher's note Springer Nature remains neutral with regard to jurisdictional claims in published maps and institutional affiliations.



Open Access This article is licensed under a Creative Commons Attribution 4.0 International License, which permits use, sharing, adaptation, distribution and reproduction in any medium or format, as long as you give appropriate credit to the original author(s) and the source, provide a link to the Creative Commons licence, and indicate if changes were made. The images or other third party material in this article are included in the article's Creative Commons licence, unless indicated otherwise in a credit line to the material. If material is not included in the article's Creative Commons licence and your intended use is not permitted by statutory regulation or exceeds the permitted use, you will need to obtain permission directly from the copyright holder. To view a copy of this licence, visit <http://creativecommons.org/licenses/by/4.0/>.

© The Author(s) 2022